Bulletin of Engineering Geology and the Environment (2019) 78:5905–5917
https://doi.org/10.1007/s10064-019-01483-5

ORIGINAL PAPER

Stress-dependent anisotropy index of strength and deformability of jointed rock mass: insights from a numerical study

Na Wu[1] · Zheng-zhao Liang[1] · Ying-chun Li[1] · Hong Li[1] · Wan-run Li[1] · Mei-li Zhang[1]

Received: 24 October 2018 / Accepted: 11 February 2019 / Published online: 28 February 2019

Abstract

Understanding the anisotropic behavior of jointed rock mass subjected to various confining pressures is crucial for designing, evaluating the performance and assessing the stability of rock engineering structures. We report here our numerical investigation of the response of stress-dependent anisotropy of a jointed rock mass sourced from the weakly weathered zone of the water inlet slope of the Xiaowan Hydropower Station, China. The finite element method (FEM) that incorporates material heterogeneity and joint network was utilized. Two-dimensional models were established based on the Monte-Carlo method and loaded in different rotational angles with changing confining pressures at the representative elementary volume (REV) size (14 × 14 m). The stress–strain behaviors, failure patterns, deformation modulus and peak strength of the REV models exhibited noticeable stress dependency and directionality. The cohesive strength was anisotropic, whereas there was only an insignificant change in the friction angle with changes in the rotational angle. The effect of confining pressure on the anisotropy index of the deformation modulus was negligible, while the anisotropy index of peak strength decreased gradually with confining pressure. Based on these results, we conclude that stress conditions need to be considered for accurate prediction of the mechanical behavior of a jointed rock mass.

Keywords Confining pressure · Anisotropy index · Strength and deformability · Jointed rock mass

Introduction

Rock masses in practical engineering works generally contain non-uniform and non-regular joints of varying sizes, orientations and locations. The presence of joints in rock mass is associated with a high scale effect (Wu and Kulatilake 2012; Bahaaddini et al. 2014; Wang et al. 2016) and anisotropy (Kohl et al. 1995; Al-Harthi 1998; Kim et al. 2012). Anisotropy is one of the distinct mechanical properties of jointed rock mass and is influenced not only by the geometric features of the joint systems, but also by the state and evolution of the in situ stress fields of the study zone. Confining pressure can contribute significantly to the strength and deformability of anisotropic rocks (Singh et al. 2015) and is a particularly significant factor in various fields of safety assessments of rock engineering projects, such as rock slopes, dam foundations and underground excavations (Kulatilake et al. 2004). Therefore, it is necessary to evaluate and quantify the effects of stress on the anisotropic characters of strength and deformability of jointed rock mass.

The effects of confining pressure on the mechanical parameters of the rock mass of anisotropic rock samples have been effectively reviewed in laboratory measurements (Attewell and Sandford 1974; Tiwari and Rao 2007; Gonzaga et al. 2008; Sahoo 2011; Maji and Sitharam 2012; Fan et al. 2017). Chappell (1990) studied the effect of in situ stresses on anisotropic rock mass and showed that rock mass modulus is very sensitive to in situ stresses. Kumar (2006) concluded that the strength of specimens for a given orientation increases nonlinearly with increasing confining pressure. One of the most important advantages of conducting laboratory experiments in this field is that more accurate results can be obtained on the influence of confining pressure on the anisotropy of strength and deformability of rocks. However, laboratory experiments are generally not adequate to estimate experimentally the variability of anisotropic mechanical parameters of jointed rock mass due to the scale effect of the samples at field scales (Bieniawski

✉ Zheng-zhao Liang
LiangZZ@dlut.edu.cn

[1] State Key Laboratory of Coastal and Offshore Engineering, Dalian University of Technology, Dalian 116024, China

1968; Singh and Rao 2005). Furthermore, such experiments are expensive and impractical for studying complex jointed rock mass (Kulatilake et al. 1994; Baghbanan 2008).

With the rapid growth of computing capacity, numerical modeling provides an effective means to facilitate an improved understanding of the stress-dependent mechanical properties of jointed rock mass (Min and Jing 2004; Bidgoli et al. 2013; Bidgoli and Jing 2015; Alshkane et al. 2017). Yang et al. (2015a) used the finite element method (FEM) to examine the dependency of strength on confining pressure based on 12-m models. They found that strength increases with confining pressure and varies with study direction. Khani et al. (2013) used the discrete element method (DEM) and determined the confined pressure dependency of elastic strength of a fractured rock mass. These authors showed that elastic strength increases with increasing confining pressure and that elasto-plastic behaviors follow a strain-hardening trend in the stress–strain curves. Bidgoli and Jing (2014) investigated the strength and deformability of fractured rocks with changing confining pressures using the DEM. Their results indicated that the strength envelopes and elastic deformability parameters of discrete element models show significant anisotropy under different confining pressures. The above-mentioned studies reveal that confining pressure plays a significant role in the strength and deformation parameters of an anisotropic rock mass.

The ratio between the maximum and minimum anisotropic parameters of a rock mass is defined as the anisotropy index and used to quantify the anisotropy degree of a rock mass. The anisotropic degree of rock mass is generally sensitive to confining pressure. A large number of studies have been carried out on the anisotropic parameters of rock masses, with many of these focusing n on sedimentary and metamorphic rocks, such as phyllite, slate and sandstone (Ramamurthy et al. 1993; Behrestaghi et al. 1996; Kumar 2006; Zhang et al. 2011, 2013; Fereidooni et al. 2016; Xu et al. 2018). The results of these studies show that the anisotropic ratio of sedimentary and metamorphic rocks decreases with increasing pressure. However, little attention has been paid to the anisotropic parameters of complex jointed rock mass. Different rock materials may show different responses in various confining pressures. Therefore, the stress-dependent anisotropy index of jointed rock mass needs further investigation to determine whether it is necessary to consider anisotropy before certain engineering operations are initiated. Furthermore, the model size for numerical experiments should be properly established so that the overall properties of rocks at field scales are statistically representative. Consequently, the representative elementary volume (REV) size of the numerical model should be evaluated (Jing and Hudson 2002; Esmaieli et al. 2010) before starting on any study of the mechanical properties of jointed rock mass associated with stress effects.

Here we report our attempt to examine the influence of confining pressure on the anisotropy of complex jointed rock mass, with the aim to gain a better understanding of the mechanical behaviors of the rock. We used the jointed rock mass of the weakly weathered zone of the water inlet slope of the Xiaowan Hydropower Station, China as study material and a FEM in which a wide variety of joint distributions were applied. First, a stochastic two-dimensional discrete fracture network (DFN) model was established using the field joint data of the slope of the powerhouse intake and the Monte Carlo method. The REV size of the jointed rock mass was obtained in the uniaxial compression tests. A set of biaxial compression experiments was then loaded in different rotational angles at REV size with changing confining pressures. The influence of confining pressure on the anisotropic degree of the jointed rock mass is discussed in quantitative terms.

Numerical modeling

Description of the Realistic Failure Process Analysis code

The computer code used in this research is the Realistic Failure Process Analysis (RFPA) code, which was developed based on the FEM. It is a powerful numerical tool to model non-linear deformability by introducing the heterogeneity of material properties into the model. It is also a numerical stress analysis tool that can handle discontinuous mechanics problems of heterogeneous materials using the continuum mechanics model by incorporating the reduction of material parameters after element failure. In RFPA, the numerical model is made up of numerous mesoscopic elements, and the four-node isoparametric elements are used to describe the basic element which is considered to be elastic and isotropic. In order to consider the heterogeneity of the numerical model, mechanical parameters of the mesoscopic elements, such as elastic modulus, strength and Poisson's ratio, are assumed to conform to a Weibull distribution (Weibull 1951), as defined by the following probability density function:

$$f(u) = \frac{m}{u_0}\left(\frac{u}{u_0}\right)^{m-1} exp\left(-\frac{u}{u_0}\right)^{m} \quad (1)$$

Where u is the specific mechanical parameter of finite elements, such as Poisson's ratio or the elastic modulus; u_o is the scale parameter related to the average value of the finite element parameter; m is the homogeneity index that can describe the degree of heterogeneity that determines the shape of the distribution function. Generally, a larger m implies more heterogeneity and vice versa. The heterogeneous medium produced by the computer is analogous to a real specimen tested in the laboratory, and so it is often deemed the numerical specimen. More details on the heterogeneity index m are available in Tang (1997).

In RFPA, the elastic damage constitutive law is applied to describe the stress–strain curve of each mesoscopic element. Initially, all mesoscopic elements of the numerical model are considered to be elastic and their properties are defined by the parameters of the elastic modulus and Poisson's ratio. Correspondingly, the stress–strain curve of the mesoscopic element is linearly elastic until the given damage threshold is reached, and then the elastic modulus of the element degrades gradually with the development of damage (Liang et al. 2004). The elastic modulus of damaged material can be described as follows:

$$E = (1-D)E_0 \tag{2}$$

where E and E_0 represent the elastic modulus of the damaged and undamaged elements, respectively, and D is the damage variable representing the degree of damage. It should be noted that the elements of the numerical model are assumed to be isotropic, therefore the E, E_0 and D are all scalars.

In the RFPA, the maximum tensile strain (or stress) criterion and the Mohr–Coulomb (M-C) criterion are chosen as the damage thresholds when the element is damaged. The constitutive relationship illustrated in Fig. 1 is adopted for the two failure modes. Generally, the maximum tensile strain (or stress) criterion takes the higher priority to determine whether the element is damaged or not. If the element is not damaged in tensile mode, the M-C criterion is then used to assess whether the element is damaged in shear modes. Correspondingly, the damage variable D is calculated when the different damage thresholds are adopted, respectively. Failure modes have been studied in detail by Zhu and Tang (2004) and Tang et al. (2005). Here, we provide a brief summary.

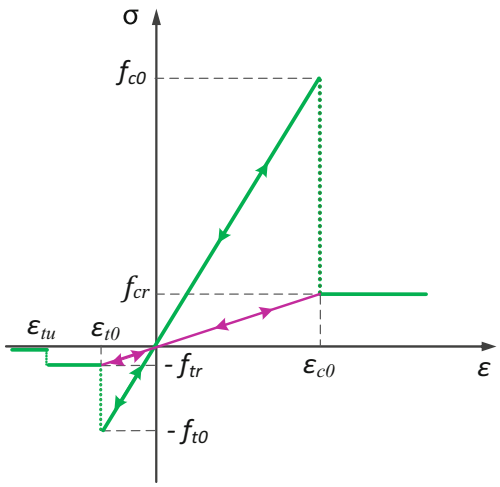

Fig. 1 Elastic-brittle damage constitutive law of elements under uniaxial stress. f_{c0}, f_{cr}, f_{t0} and ftr denote uniaxial compressive strength, residual uniaxial compressive strength, uniaxial tensile strength and residual tensile strength, respectively; ε_{c0}, ε_{t0} and ε_{tu} represent uniaxial compressive strain, tensile strain at the elastic limit and ultimate tensile strain of the element, respectively

If the model element is subjected to uniaxial tension state and the tensile stress in the element reaches its tensile strength, f_{t0}, then

$$\sigma_3 \le f_{t0} \tag{3}$$

where σ_3 and f_{t0} are minimum principal stress and the uniaxial tensile strength of mesoscopic element, respectively.

The constitutive relations of elasto-brittle damage with given specific residual strength is presented in the third quadrant of Fig. 1. With regard to the corresponding constitutive law where the element is damaged in tension mode, the parameter D can be expressed in Eq. (4) as:

$$D = \begin{cases} 0, & \varepsilon > \varepsilon_{t0} \\ 1-\dfrac{\lambda\varepsilon_{t0}}{\varepsilon}, & \varepsilon_{tu} < \varepsilon \le \varepsilon_{t0} \\ 1, & \varepsilon \le \varepsilon_{tu} \end{cases} \tag{4}$$

where λ is the residual strength coefficient and $\lambda = f_{tr}/f_{to}$, and f_{to} and f_{tr} are the uniaxial tensile strength and residual tensile strength, respectively; ε_{to} is the strain at the elastic limit, while ε_{tu} is the ultimate tensile strain of the element. The ultimate tensile strain is defined by $\varepsilon_{tu} = \eta\varepsilon_{to}$, where η is the ultimate strain coefficient.

Additionally, the constitutive described before can be extended to three-dimensional stress fields according to the method of extending a one-dimensional constitutive law under uniaxial tensile stress to a multiaxial stress condition (Mazars and Pijaudier-Cabot 1989). In a multiaxial stress state, the tensile damage still occurs when the equivalent maximum tensile strain $\overline{\varepsilon}$ reaches the above threshold strain ε_{t0}. The equivalent principal strain $\overline{\varepsilon}$ is described in Eq. (5):

$$\overline{\varepsilon} = -\sqrt{\langle -\varepsilon_1 \rangle^2 + \langle -\varepsilon_2 \rangle^2 + \langle -\varepsilon_3 \rangle^2} \tag{5}$$

where ε_1, ε_2 and ε_3 are three principal strains; the term within the angular bracket is a function expressed in Eq. (6):

$$\langle x \rangle = \begin{cases} x, & x \ge 0 \\ 0, & x < 0 \end{cases} \tag{6}$$

Therefore, the constitutive law for an element subjected to multiaxial stresses can be further expressed in Eq. (4) by substituting the strain ε with the equivalent strain $\overline{\varepsilon}$ defined by Eqs. (5) and (6). The damage variable D is then defined in Eq. (7):

$$D = \begin{cases} 0, & \overline{\varepsilon} > \varepsilon_{t0} \\ 1-\dfrac{\lambda\varepsilon_{t0}}{\overline{\varepsilon}}, & \varepsilon_{tu} < \overline{\varepsilon} \le \varepsilon_{t0} \\ 1, & \overline{\varepsilon} \le \varepsilon_{tu} \end{cases} \tag{7}$$

However, if the model elements are subjected to compressive and shear stresses, compressive softening also occurs.

Therefore, shear damage of the modeling elements is assumed to exist, and the constitutive relationship of the M-C criterion is selected as the second damage, which is described by Eq. (8):

$$\sigma_1 - \frac{1+sin\varphi}{1-sin\varphi}\sigma_3 \geq f_{c0} \tag{8}$$

where σ_1 and σ_3 are the maximum and minimum principal stress values, respectively. In RPFA, compressive stress is positive and tensile stress is negative. In addition, f_{co} and φ are the uniaxial compressive strength (UCS) and internal friction angle of the mesoscopic element, respectively. With regard to the corresponding constitutive law where the element is damaged in shear stress, the parameter D under uniaxial tension can be expressed in Eq. (9):

$$D = \begin{cases} 0, & \varepsilon < \varepsilon_{c0} \\ 1 - \dfrac{\lambda\varepsilon_{c0}}{\varepsilon}, & \varepsilon \geq \varepsilon_{c0} \end{cases} \tag{9}$$

where λ is also the residual strength coefficient, and $\lambda = f_{cr}/f_{co}$ is assumed to be true when an element is under uniaxial tension or compression. Among these, f_{co} and f_{cr} are the UCS and residual UCS, respectively, as shown in Fig. 1; ε_{c0} is the strain at the peak compressive principal stress.

If an element is under multiaxial stress and its stress condition satisfies the M-C criterion, the element can still be damaged in the shear mode. The effect of intermediate principal stresses on the damage process should be considered in this model. When the M-C criterion is satisfied, the minimum principal strain (or maximum compressive principal strain) ε_{c0} can be obtained at the peak of the maximum principal stress (or maximum compressive principal stress) value, as follows:

$$\varepsilon_{c0} = \frac{1}{E_0}\left[f_{c0} + \frac{1+sin\varphi}{1-sin\varphi}\sigma_3 - \mu(\sigma_1+\sigma_2)\right] \tag{10}$$

where ν, E_o, f_{co} and φ are Poisson's ratio, original elastic modulus element, UCS and internal friction angle of the numerical element, respectively. In this regard, it is assumed that shear damage evolution is only induced by the maximum compressive principal strain ε_1. Correspondingly, the damage variable D can be easily obtained by replacing the uniaxial compressive strain ε_{c0} in Eq. (9) with the maximum compressive principal strain ε_1. Consequently, the parameter D under triaxial stress states for shear damage as follows:

$$D = \begin{cases} 0, & \varepsilon_1 < \varepsilon_{c0} \\ 1 - \dfrac{\lambda\varepsilon_{c0}}{\varepsilon_1}, & \varepsilon_1 \geq \varepsilon_{c0} \end{cases} \tag{11}$$

In summary, the damaged elastic modulus of each element at the stress or strain state can be calculated from the above expression on the damage variable D together with Eq. (2), which is generally named the damage evolution law in damage mechanics. Further, the initial element is linearly elastic and no damage occurs, i.e. $D = 0$, so the damage variable D ranges from 0 for the undamaged element to 1 for the complete failure element.

RFPA can not only take into account the heterogeneity of rock mass at the micro- and macroscopic levels, but also capture the key behaviors of rock deformation and failure, including the initiation and development of cracks under different loading conditions and loading stages, and reproduce the localization of deformation, stress redistribution, strain softening, failure modes, etc. This code has been widely used to simulate mechanical properties in rocks (Tang 1997; Zhu and Tang 2004). The validity and reliability of the RFPA code have been assessed in a number of typical laboratory tests on idealized jointed rock samples to evaluate the anisotropic behavior of jointed rock samples (Tang et al. 2001; Xu et al. 2013; Yan et al. 2013; Liang et al. 2004). In addition, the RFPA code has been widely applied to investigate slope stability (Li LC et al. 2009; Liu et al. 2017), scale effect and anisotropy (Yang et al. 2015b; Zhou et al. 2018) of jointed rock mass in a number of engineering fields. Therefore, the RFPA can be considered to be an effective tool to investigate the anisotropic behavior of jointed rock mass. In addition, as a FEM-based method, axial stress, axial strain and equilibrium are calculated in the RFPA code in the same manner as in other finite element methods.

Determination of REV size

The Xiaowan Hydropower Station is located in the middle reaches of the Lancang river between Nanjian county (Dali prefecture) and Fengqing county (Lincang city, Yunnan province). The water inlet slope of the Xiaowan Hydropower Station is located on the right size of Dachunshugou. The foundation elevation of the water inlet platform is 1140 m, and the elevation of the gate well platform is 1245 m. The lithology of the rock body in the water inlet slope is mainly long gneiss and black cloud granite gneiss. There is no large fault in the area, and the stability of the slope is mainly controlled by small faults and joint developed in the rock mass. According to the rock mass weathering degree, the water inlet slope is divided into a strong weathering zone, weak weathering zone and micro-new rock mass in the direction from the surface to the interior. Of these, the weakly weathered zone of the water inlet slope of the Xiaowan Hydropower Station contains three sets of joints, which were estimated by Wang et al. (2010) in a field investigation using the scanline method (see Table 1). In order to characterize the stochastic fracture system for the numerical simulation, a 30 × 30-m DFN model was generated based on the probability model and Monte Carlo method.

REV is a critical value beyond which the mechanical parameters of jointed rock mass tend to stabilize as model size

Table 1 The probability distribution of joint geometric parameters in the weakly weathered zone of the water inlet slope of the Xiaowan Hydropower Station. There are three joint sets (J_A, J_B and J_C) in this zone

Joint set	Dip angle (°)			Trace length (m)			Spacing (m)		
	Distribution pattern[a]	Mean value	Standard deviation	Distribution pattern[a]	Mean value	Standard deviation	Distribution pattern[a]	Mean value	Standard deviation
J_A	I	80.26	9.91	II	2.54	1.39	III	0.3	0.3
J_B	I	89.3	9.52	II	1.56	1.01	II	0.31	0.44
J_C	I	42.88	6.54	II	1.52	0.87	II	0.29	0.29

Values in table are from in a field investigation using the scanline method conducted by Wang et al. (2010)

[a] I represents normal distribution, II represents logarithmic normal distribution and III represents negative exponential distribution, respectively

increases. The existence of REV is capable of reproducing the representative mechanical property of jointed rock mass, based on which the continuous-media theory can be applied (Pariseau et al. 2008; Li JH et al. 2009). In order to determine the REV size of jointed rock mass, square models (n = 10) with the size ranging from 2 to 20 m, each with an increment of 2 m, were used to investigate the scale effect in the uniaxial compression tests. For each square model, six rotational angles θ (θ = 0°, θ = 30° to θ = 150°) in the counter-clockwise direction were chosen based on the suggestions of previous studies (Bidgoli and Jing 2014; Yang et al. 2015a; Kumar and Verma 2016), as shown in Fig. 2. The blue lines in Fig. 2 represent generated joints. The concentric squares formed by black lines represent research regions for computational FEM models. The RFPA^{2D} code was adopted and the basic mechanical properties of intact rock in RFPA2D were acquired based

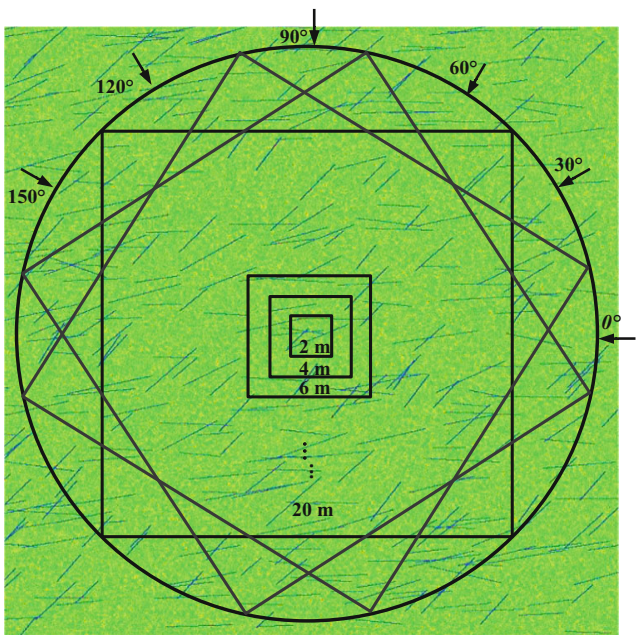

Fig. 2 Illustration of the finite element method (FEM) model used to study the mechanical properties of jointed rock mass. Blue lines represent generated joints; concentric squares formed by black lines represent research regions for computational FEM models

on the results of field and laboratory tests. In the RFPA, the joint elements are simplified to be a kind of special intact rock material. The mechanical parameters of the joint include UCS, elastic modulus, friction angle, among others. Generally, the mechanical parameters of joints are relatively lower than those of intact rocks, and the joint parameter selection would influence the analysis results (Wu et al. 2017). However, the ratios of mechanical properties between joint and intact rock have not yet been reported. In previous studies, the values of UCS and elastic modulus of joint have generally been set within the range of 1–20% (Kemeny 1991; Pariseau et al. 2008; Li et al. 2011; Yang et al. 2015b; Zhou et al. 2018). Additionally, in our study the magnitude of joint parameters is seemly less important because it is the impact of joint on the trend of the calculation results that is the focus of our research. We set the ratios of elastic modulus and UCS to 4.36 and 4.22%, respectively. The properties of intact rock and joint are listed in Table 2. The top of the FEM model was applied as an axial displacement-controlled constant load per step until model failure. The strain rate of 2.0e-5 per step was used in the numerical simulation based on the suggestions of Yang and Jing (2011).

The variations in UCS with FEM model sizes for six rotational angles are shown in Fig. 3. The results indicate that the variation trend of UCS with FEM model size is similar for each rotational angle. The UCS first increases and then gradually decreases until it tends to stabilize as FEM size increases. It is clearly seen that the values of the UCS for six rotational angles remain almost unchanged when the FEM model size is greater than 14 × 14 m. Therefore, the REV of the jointed rock mass is determined to be 14 × 14 m.

Biaxial compression tests

To study the effects of confining pressure on the anisotropic behaviors of jointed rock mass, we constructed six square models at REV size (14 × 14 m) from the DFN model at angles of 0° to 180° at an interval of 30° in the counter-clockwise direction under different levels of confining pressure. The mechanical parameters of intact rock and joint under biaxial

Table 2 The mechanical parameters for rocks and joints used in the compression numerical tests

Material type	Heterogeneity index	Elastic modulus (GPa)	Uniaxial compressive strength (MPa)	Friction angle (°)	Poisson's ratio
Rock	5	42.2	105.2	51	0.28
Joint	2	1.84	4.44	28	0.34

compression test are the same as those in the uniaxial compression test, as listed in Table 2. A typical illustration of set-ups and boundary conditions of the biaxial compression tests is provided in Fig. 4. In the biaxial compression tests, the bottom of the REV model was fixed in the *y*-direction, the confining pressures were applied on the vertical boundary surfaces of the REV model and a constant axial displacement-controlled load (U) at a strain rate of 2.0e-5 per step (0.28 mm/step) was applied to the top of the REV model until failure occurred. In addition, the various confining pressures (P) were in turn set at the values of 0, 0.5, 1.0, 1.5, 2.0 and 2.5 MPa, respectively.

Results and analysis

Stress–strain behaviors and failure patterns of jointed rock mass under confining pressure

The axial stress–strain curves and failure patterns of the REV models for six rotational angles under different confining pressures are shown in Figs. 5 and 6. Figure 5 shows that the trend in axial stress–strain behaviors of the REV models for each rotational angle is closely similar under the various confining pressures. During the initial loading stage, the REV model deforms linearly and elastically before the axial stress reaches the yield strength, which is defined as the stress point at which the elastic deformation starts changing into the plastic deformation on a stress–strain curve. As loading further increases, the REV models follow an elasto-plastic deformation behavior up to the peak strength and show a stress-hardening manner. These results are in agreement with those of previous studies (Bidgoli et al. 2013; Yang et al. 2015a). Finally, the axial stress–strain curve constantly decreases with multi-peak strengths and exhibits strain-softening behavior. This similar trend in axial stress–strain behavior at different rotational angles can be explained by the failure patterns of the REV models under different confining pressures, as shown in Fig. 6. It can be seen that the REV models for 0° rotational angle mainly show tensile failure along the pre-existing joints and shear failure at the tips of the pre-existing joints under various confining pressures and that the stress–strain curve is generally related to the failure process of the model. Moreover, the results also show that the REV size of the model, 14 × 14 m, is adequate for studying the average strength and deformability of the jointed rock mass under study.

Furthermore, the slope of the stress–strain curve during the elastic deformation stage and the peak strength of the REV models increase with increasing confining pressure, as shown in Fig. 5. The mechanical behaviors of the REV models also become increasingly ductile as confining pressure increases (Attewell and Sandford 1974; Rao 1984). This behavior can be explained in terms of the distribution of microcrack in the REV models with the increasing of confining pressure, as shown in Fig. 6. When the confining pressure is small, i.e. 0, 0.5 and 1 MPa, the microcracks initiate and propagate along the flaw of the models. However, the microcracks are only

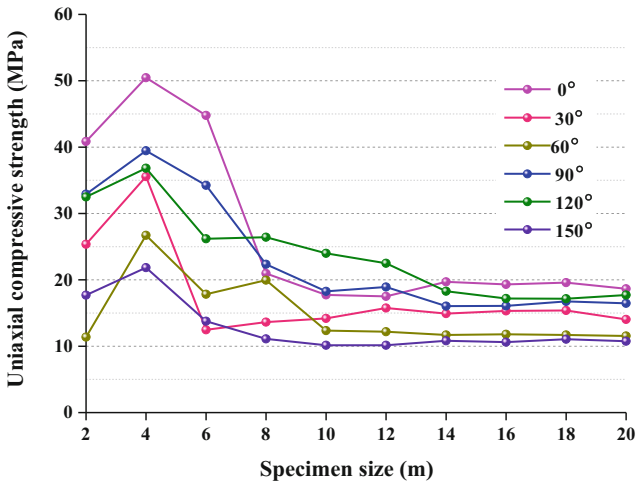

Fig. 3 Variation in uniaxial compressive strength (UCS) with changes in FEM model size for six different rotational angles

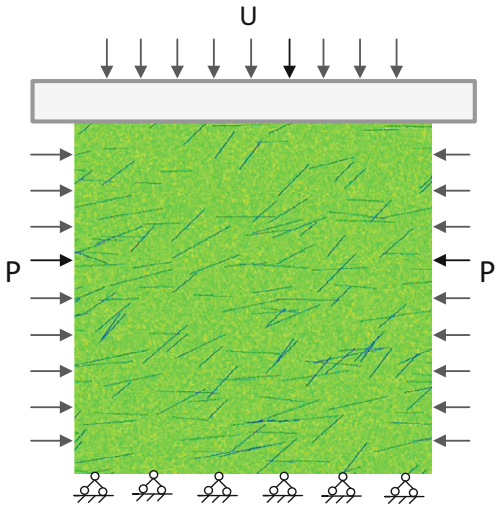

Fig. 4 Typical set-ups and boundary conditions for biaxial compression tests. *P* Confining pressure, *U* axial displacement-controlled load

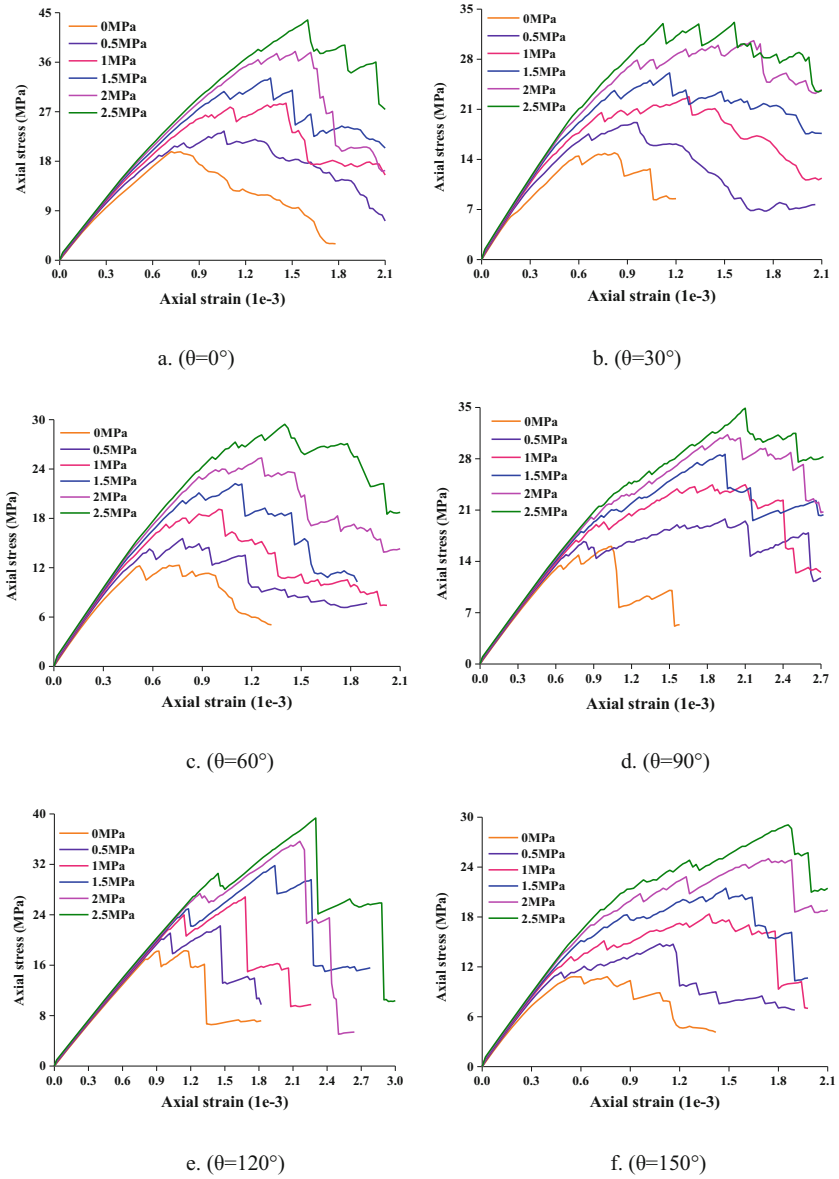

Fig. 5 Axial stress–strain curves of the rotated representative elementary volume (REV) models under different confining pressures

generated along the upper-left and lower-right joints of the REV models, and the other joints and lateral dilation of the REV models are restrained as confining pressure further increases.

Anisotropy behaviors of stress–strain and failure patterns of jointed rock mass

Figure 7, as an example, shows the axial stress–strain curves of the rotated REV models under a confining pressure of 1.5 MPa, and the existence of joints has an important impact on the macro behavior of the rock mass (Fan et al. 2018; Zhang et al. 2018). The numerical results indicate that the axial stress–strain curves of the REV models loaded in various rotational angles have significant anisotropy and directionality. The main reason for this significant anisotropy and directionality is the complex geometry of the joint system. Moreover, the slopes of the straight line portions of the axial stress–strain, peak strain and peak strength change with rotational angle.

The fracture patterns and micro crack distributions of the rotated REV models under a confining pressure of 1.5 MPa are shown in Fig. 8. According to the distribution of micro-fractures in the REV models, multiple failure planes are observed along the pre-existing joints whereas the anisotropy of macro failure patterns of the REV models was found to be significant. When the rotational angles are at 0°, 30°, 60° and 120°, respectively, the REV models are damaged by the shear zones running through the whole models and follow a shear failure pattern. However, the distributions of the shear zones in the REV models are dominated by the joint direction. For the 90° rotational angle, the damaged zones occupy the lower-left and upper-right corners of the REV model, and the REV model mainly shows the combined action of a shear-tension

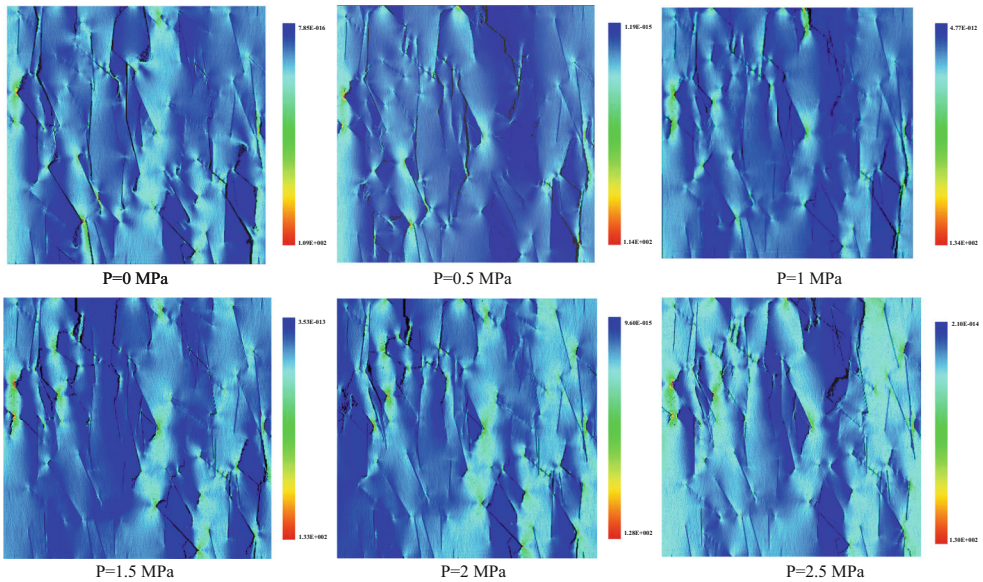

Fig. 6 The failure patterns of the REV models at 0° rotational angle under various confining pressures (*P*)

failure pattern. For the 150° rotational angle, the micro-cracks mainly occur along the pre-existing joints that nearly parallel the model diagonals, and the REV model mainly shows surface failure. Therefore, the distribution and direction of joints have a dominating influence on the failure patterns of jointed rock mass. Furthermore, the anisotropy behaviors of jointed rock mass, as shown in Fig. 7, might be explained by the anisotropy of the failure patterns of the rotated REV models.

Equivalent strength and deformation parameters of jointed rock mass under confining pressure

We obtained the mechanical parameters of the deformation modulus and peak strength in this study. Among these, deformation modulus was taken as the ratio of stress to strain of the stress–strain curve during the elastic deformation stage, and the peak strength was obtained as the maximal axial stress of the stress–strain curve during the loading process.

Variations in the deformation modulus and peak strength as a function of confining pressures for different rotational angles are shown in Figs. 9 and 10. It can be seen that a higher confining pressure is correlated with higher deformation modulus and peak strength, results which agree with those of previous studies. Moreover, the deformation modulus increases linearly with increasing confinement, whereas the same increase in confining pressure causes a different increase in peak strength for various rotational angles. Engineering applications in various in situ stress conditions should consider this aspect for design and analysis.

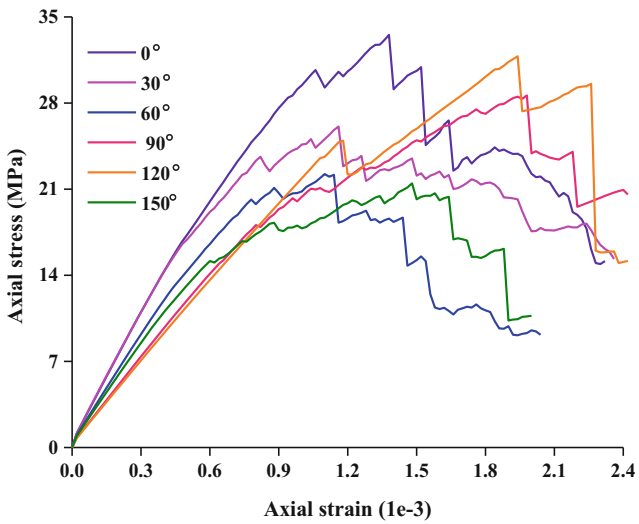

Fig. 7 Axial stress–strain curves of the rotated REV models under a confining pressure of 1.5 MPa

Anisotropy of equivalent strength and deformation parameters

The relation of the deformation modulus and peak strength as a function of rotational angles under different confining pressures are shown in Figs. 11 and 12, respectively. The deformation modulus and the peak strength have obvious anisotropy and directionality, due to the different orientations of joints relative to the loading direction. As shown in Fig. 11, the deformation modulus first increases slightly with increases in the rotational angle from 0° to 30°; this is followed by a decrease in the deformation modulus from 0° to 120° rotational angles and an increase from 120° to 180° rotational angles. The property of the deformation modulus exhibits a shoulder-shaped form based on the classification of Ramamurthy et al. (1993). For groups at different confining pressures, the maximum and minimum deformation modulus are observed at a rotational angle of 30° and 120°, respectively.

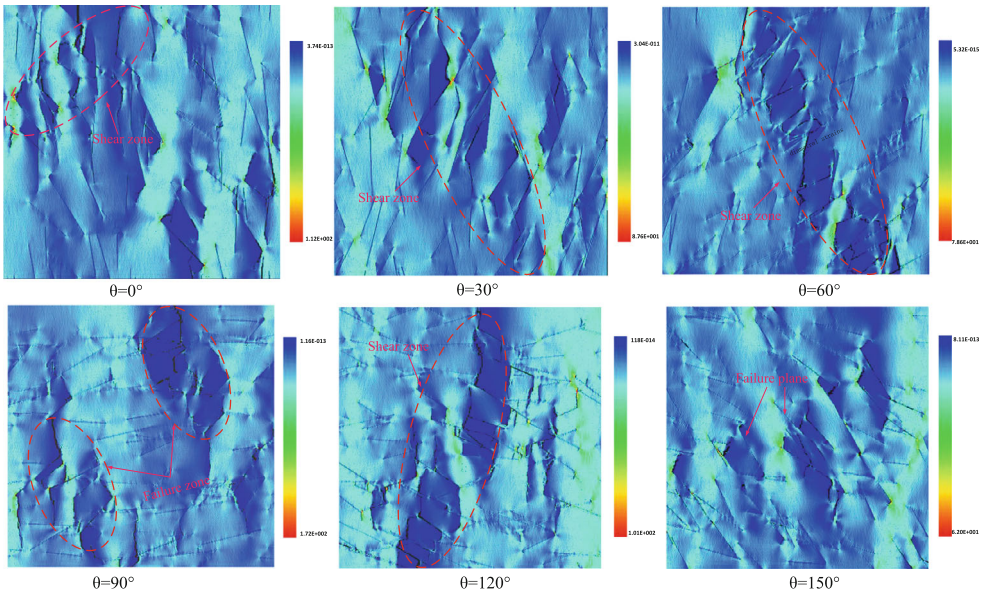

Fig. 8 The failure patterns of the rotated REV models under a confining pressure of 1.5 MPa

As plotted in Fig. 12, peak strength decreases initially at a rotation angle of between 0° and 60°, then increases at a rotation angle of between 60° and 120° and finally decreases and increases again when the rotation angle is between 120° to 180°. The property of peak strength displays a undulatory type based on the classification of Ramamurthy et al. (1993). The maximum and minimum values of the peak strength are at around 0° and 150° rotational angles for groups with different confining pressures, respectively.

The equivalent cohesive strength and friction angle of the rotated REV models can be reasonably reviewed by fitting numerical experiment data based on M-C and Hoek–Brown (H-B) (Hoek and Brown 1980) strength criteria. Both of these strength criteria are widely accepted in the international rock mechanics community, but the M-C strength criterion is the better criterion for jointed rock mass under low confining pressure (Bidgoli et al. 2013; Bidgoli and Jing 2015). Hence, the equivalent cohesive strength and friction angle of the rotated REV models are determined based on linearly M-C strength criterion.

The M-C strength criterion of a rock may be written as:

$$\frac{\sigma_1}{\sigma_3} = \frac{1+\sin\theta}{1-\sin\theta} + \frac{\frac{2c\cos\theta}{1-\sin\theta}}{\sigma_3} \tag{12}$$

where c is the cohesive strength; θ is the friction angle; σ_1 is the major principal stress at failure; and σ_3 is the confining pressure.

Figures 13 and 14 show the distributions of cohesive strength and friction angle with the rotational angles, when the M-C strength criterion w adopted. It can be seen that the jointed rock mass has obvious directionality and anisotropy in

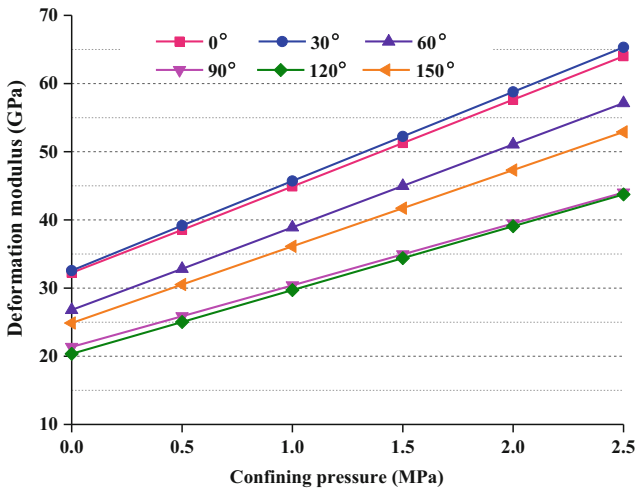

Fig. 9 Influence of confining pressure on the deformation modulus at various rotational angles

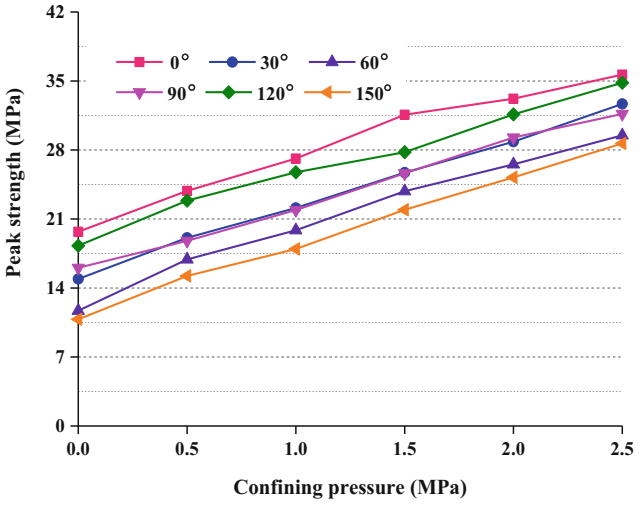

Fig. 10 Influence of confining pressure on the peak strength at various rotational angles

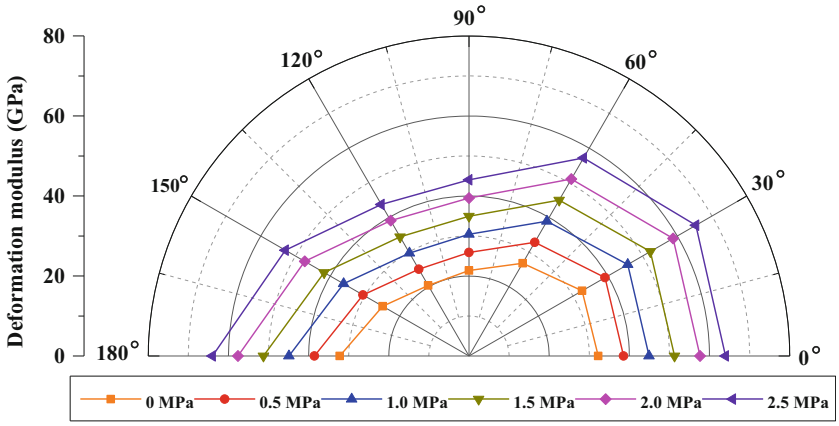

Fig. 11 Anisotropy of the deformation modulus under various confining pressures

cohesive strength. However, the change in the friction angle with rotational angle is insignificant. The main reason for the results is the slight changes in the slope angles of the fitted linear curves in Fig. 10 based on M-C strength criterion. This result agrees with that of Bidgoli and Jing (2014). The numerical models show that the maximum and minimum cohesive strengths are 3.471 and 1.667 MPa at around 90° and 150° rotational angles, respectively. Moreover, the maximum and minimum friction angles are close to 54.015° and 47.795° at around 0° and 60° rotational angles, respectively.

Effect of confining pressure on the anisotropy index

The anisotropy index is an important evaluation criterion to quantify the anisotropy degree of rock mass. In order to analyze the impact of confining pressure on the anisotropy index of jointed rock mass, we must first establish the anisotropy index:

$$CV_{\alpha j} = \frac{\alpha_{ij}}{\alpha_{ij(\min)}} \tag{13}$$

where $CV_{\alpha j}$ is the anisotropy index represented in terms of deformation modulus or peak strength of the REV model under the intermittent confining pressure j (0 MPa, 0.5 MPa to 2.5 MPa); α_{ij} is the deformation modulus (or peak strength) when the intermittent rotational angle i (0°, 30°,…, 150°) and the corresponding confining pressure is j; $\alpha_{ij(\min)}$ is the minimum deformation modulus (or peak strength) among α_{ij}. It can be seen from Eq. (13) that the smallest anisotropy index, with a magnitude of 1, exists when $\alpha_{ij(min)} = \alpha_{ij}$; the value of 1 is a reference value to evaluate to which extent the confining pressure impacts on the anisotropic behavior of jointed rock mass. The greater the anisotropy index is, the stronger the anisotropy becomes.

Figures 15 and 16 show the variation in the anisotropy indexes of deformation modulus and peak strength, respectively, as a function of confining pressure for different rotational angles. As plotted in Fig. 15, the results indicate that the anisotropy index of the deformation modulus has a decreasing trend with increases in confining pressure, with the exception of at a rotation angle of 120°, when the value is equal to 1. An interesting feature is that changes in the anisotropy index of the deformation modulus are smaller than the relative experimental errors (8%) with increases in confining pressure. Thus, the effect of confining pressures on the anisotropy index of the deformation modulus can be neglected. When various rotational angles are compared, the anisotropy index of the deformation modulus shows directionality and anisotropy. The maximum and minimum anisotropy indexes of the

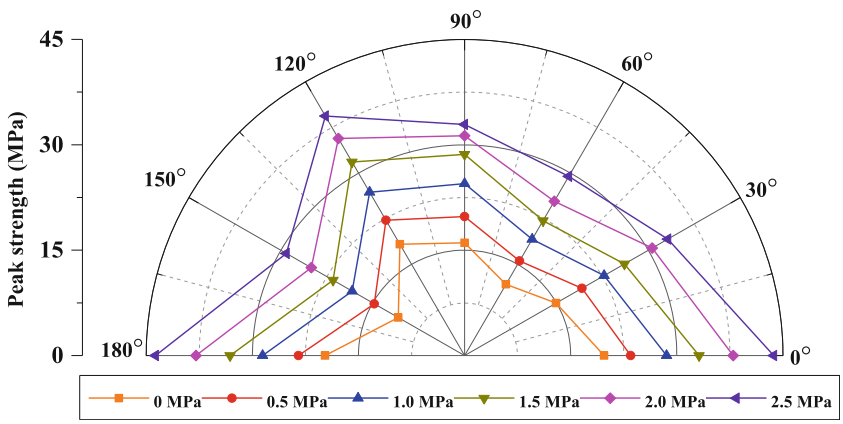

Fig. 12 Anisotropy of peak strength under various confining pressures

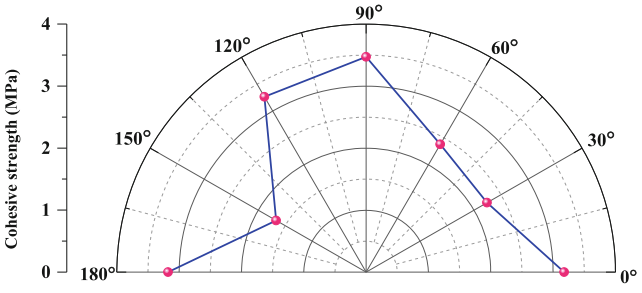

Fig. 13 Distribution of cohesive strength for the rotated REV models

deformation modulus under a confining pressure of 2.5 MPa are about 1.493 and 1 at a rotational angle of approximately 30° and 120°, respectively.

As seen in Fig. 16, the anisotropy index of the peak strength moves in an obvious downward trend with increases in confining pressure, with the exception of at a rotational angle of 150° rotational, when the value is equal to 1. However, the changes in the reduction trend are moderate. At 0° and 60° rotational angles, the anisotropy index of the peak strength first shows a large drop and then remains almost constant with increasing confining pressure. Furthermore, the anisotropy index of the peak strength first decreases gradually, then remains almost unchanged before finally decreasing again at rotational angles of 30°, 90° and 120°, respectively, as confining pressure increases. When various rotational angles are compared, the anisotropy index of the peak strength also shows directionality and anisotropy. In relative terms, the maximum and minimum anisotropy indexes of the peak strengths under a confining pressure of 2.5 MPa are about 1.505 and 1 at a rotational angle of approximately 0° and 150°, respectively.

Discussion

Jointed rock mass displays significant anisotropy in uniaxial and biaxial compression tests. The mechanical parameters of jointed rock mass, such as deformation modulus and peak strength, vary with rotational angle and have obvious anisotropy and directionality under various confining pressures. The

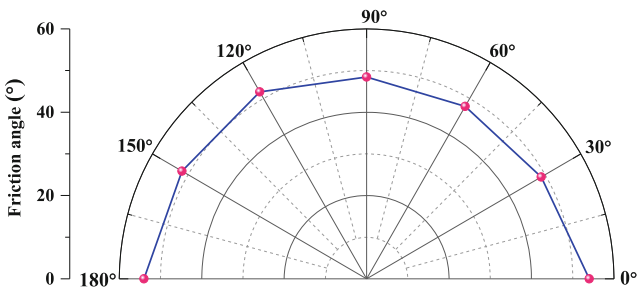

Fig. 14 Distribution of friction angle for the rotated REV models

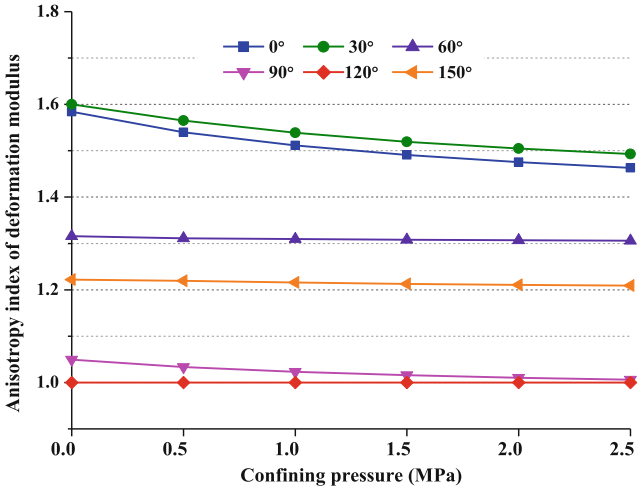

Fig. 15 Variation in the anisotropy index of deformation modulus as a function of confining pressure for different rotational angles

anisotropy index quantifies the anisotropy degree of a rock mass and this index is sensitive to confining pressure. Our simulation results show that an increase in the confining pressure reduces the anisotropic degree of jointed rock mass in terms of strength parameters, which is consistent with those of sedimentary and metamorphic rocks (Ramamurthy et al. 1993; Behrestaghi et al. 1996; Zhang et al. 2013; Fereidooni et al. 2016; Xu et al. 2018). A high confining pressure can restrain lateral dilation, enhance rock strength and encourage homogenization. However, the confining pressure has little influence on the anisotropic degree of the deformation modulus—i.e. the effect of confining pressure on the anisotropy index of the deformation modulus can be neglected. Furthermore, the mechanical parameters of jointed rock mass may be considered as isotropy when the confining pressure is sufficiently high.

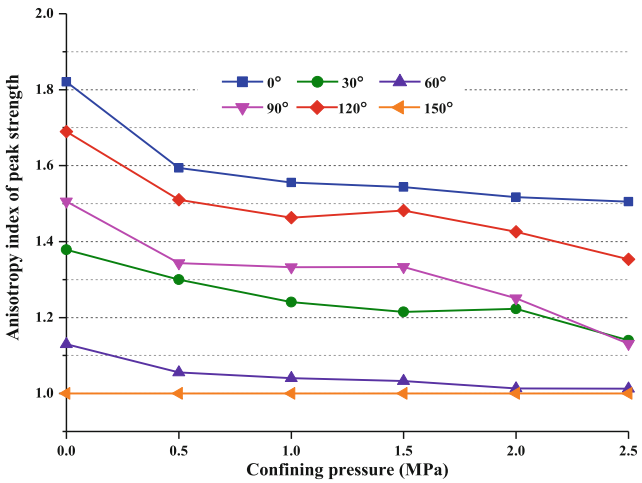

Fig. 16 Variation in the anisotropy index of peak strength as a function of confining pressure for different rotational angles

Conclusions

The effects of confining pressure on anisotropy of the strength and deformation properties of jointed rock were investigated using the DFN–FEM approach at the REV size. The method may play an important role in the anisotropy of jointed rock mass at the field scale and provides more reasonable estimations, which requires reliable fracture system characterization.

Significant scale-dependency of the peak strength of the jointed rock mass for different rotational angles was observed in uniaxial compression experiments. The REV size of jointed rock mass existed and was approximated to be 14 × 14 m.

To systematically investigate the stress-dependent anisotropy of the equivalent strength and deformation behaviors of jointed rock mass, a series of biaxial compression experiments was then carried at different rotational angles at REV size, with varying confining pressures. The results indicated that stress–strain behaviors, failure patterns, deformation modulus and peak strength exhibited significant stress dependency and anisotropy. In addition, the cohesive strength and friction angle were obtained based on the M-C strength criterion. These results clearly showed that the friction angle changed insignificantly with changes in rotational angle, while the cohesive strength exhibited significant anisotropy.

The influence of confining pressure on the anisotropic degree of jointed rock mass was quantified using an index termed the 'anisotropy index'. The results indicated that confining pressure weakened the anisotropy features of jointed rock mass. It is emphasized that the effect of confining pressures on the anisotropy index of deformation modulus can be neglected, whereas the anisotropy index of peak strength gradually decreased with increasing confining pressure. Furthermore, the anisotropy indexes of both the deformation modulus and the peak strength showed directionality and anisotropy.

The present study is based on a two-dimensional analysis, which is more suitable for plane–strain problems, such as tunnel projects with random joint sets. The effect of complex stress combinations on the anisotropy of strength and deformability of engineering rock mass demands are further revealed.

Acknowledgements This study is supported by the National key research and development program(2016YFBO201000) and the National Natural Science Foundation of China (Grant No. 51779031).

References

Al-Harthi AA (1998) Effect of planar structures on the anisotropy of ranyah sandstone, Saudi Arabia. Eng Geol 50(97):49–57

Alshkane YM, Marshall AM, Stace LR (2017) Prediction of strength and deformability of an interlocked blocky rock mass using UDEC. J Rock Mech Geotech Eng 9(3):149–160

Attewell PB, Sandford MR (1974) Intrinsic shear strength of a brittle, anisotropic rock—III: textural interpretation of failure. Int J Rock Mech Min Sci Geomech Abstr 11(11):431–438

Baghbanan A (2008) Stress and scale-dependency of hydromechanical properties of fractured rocks. Isfahan University of Technology, Isfahan

Bahaaddini M, Hagan PC, Mitra R, Hebblewhite BK (2014) Scale effect on the shear behaviour of rock joints based on a numerical study. Eng Geol 181:212–223

Behrestaghi MHN, Rao KS, Ramamurthy T (1996) Engineering geological and geotechnical responses of schistose rocks from dam project areas in India. Eng Geol 44(1–4):183–201

Bidgoli MN, Jing L (2014) Anisotropy of strength and deformability of fractured rocks. J Rock Mech Geotech Eng 6(2):156–164

Bidgoli MN, Zhao Z, Jing L (2013) Numerical evaluation of strength and deformability of fractured rocks. J Rock Mech Geotech Eng 5(6): 419–430

Bidgoli MN, Jing L (2015) Stochastic analysis of strength and deformability of fractured rocks using multi-fracture system realizations. Int J Rock Mech Min Sci 78(4):108–117

Bieniawski ZT (1968) The effect of specimen size on compressive strength of coal. Int J Rock Mech Min Sci Geomech Abstr 5(4): 325–335

Chappell BA (1990) Moduli stress dependency in anisotropic rock masses. Min Sci Technol 10(2):127–143

Esmaieli K, Hadjigeorgiou J, Grenon M (2010) Estimating geometrical and mechanical REV based on synthetic rock mass models at Brunswick mine. Int J Rock Mech Min Sci 47(6):915–926

Fan LF, Wu ZJ, Wan Z, Gao JW (2017) Experimental investigation of thermal effects on dynamic behavior of granite. Appl Therm Eng 125:94–103

Fan LF, Gao JW, Wu ZJ, Yang SQ, Ma GW (2018) An investigation of thermal effects on micro-properties of granite by X-ray CT technique. Appl Therm Eng 140:505–519

Fereidooni D, Khanlari GR, Heidari M, Sepahigero AA, Kolahi-Azar AP (2016) Assessment of inherent anisotropy and confining pressure influences on mechanical behavior of anisotropic foliated rocks under triaxial compression. Rock Mech Rock Eng 49(6):2155–2163

Gonzaga GG, Leite MH, Corthésy R (2008) Determination of anisotropic deformability parameters from a single standard rock specimen. Int J Rock Mech Min Sci 45(8):1420–1438

Hoek E, Brown ET (1980) Empirical strength criterion for rock masses. J Geotech Eng Div ASCE 106(GT9):1013–1103

Jing L, Hudson JA (2002) Numerical methods in rock mechanics. Int J Rock Mech Min Sci 39(4):409–427

Kemeny JM (1991) A model for non-linear rock deformation under compression due to sub-critical crack growth. Int J Rock Mech Min Sci Geomech Abstr 28(6):459–467

Khani A, Baghbanan A, Norouzi S, Hashemolhosseini H (2013) Effects of fracture geometry and stress on the strength of a fractured rock mass. Int J Rock Mech Min Sci 60(8):345–352

Kim H, Cho JW, Song I, Min KB (2012) Anisotropy of elastic moduli, p-wave velocities, and thermal conductivities of Asan gneiss, boryeong shale, and yeoncheon schist in Korea. Eng Geol 147-148(5):68–77

Kohl T, Evansi KF, Hopkirk RJ, Rybach L (1995) Coupled hydraulic, thermal and mechanical considerations for the simulation of hot dry rock reservoirs. Geothermics 24(24):345–359

Kulatilake PHSW, Ucpirti H, Stephansson O (1994) Effects of finite-size joints on the deformability of jointed rock at. Can Geotech J 31(3): 364–374

Kulatilake PHSW, Park J, Um JG (2004) Estimation of rock mass strength and deformability in 3-d for a 30 m cube at a depth of

485 m at Äspö hard rock laboratory. Geotech Geol Eng 22(3):313–330

Kumar A (2006) Engineering behaviour of anisotropic rocks. PhD thesis. Department of Civil Engineering, Indian Institute of Technology, Roorkee

Kumar R, Verma AK (2016) Anisotropic shear behavior of rock joint replicas. Int J Rock Mech Min Sci 90:62–73

Li JH, Zhang LM, Wang Y, Fredlund DG (2009) Permeability tensor and representative elementary volume of saturated cracked soil. Can Geotech J 46(8):928–942

Li LC, Tang CA, Zhu WC, Liang ZZ (2009) Numerical analysis of slope stability based on the gravity increase method. Comput Geotech 36(7):1246–1258

Li LC, Yang TH, Liang ZZ, Zhu WC, Tang CA (2011) Numerical investigation of groundwater outbursts near faults in underground coal mines. Int J Coal Geol 85(3–4):276–288

Liang ZZ, Tang CA, Li HX, Zhang YB (2004) Numerical simulation of the 3-D failure process in heterogeneous rocks. Int J Rock Mech Min Sci 41(3):419–419

Liu XZ, Tang CA, Li LC, Lv PF, Liu HY (2017) Microseismic monitoring and 3D finite element analysis of the right bank slope, Dagangshan Hydropower Station, during reservoir impounding. Rock Mech Rock Eng 50(7):1901–1917

Maji VB, Sitharam TG (2012) Testing and evaluation of strength and deformation behaviour of jointed rocks. Geomech Geoeng 7(2): 149–158

Mazars J, Pijaudier-Cabot G (1989) Continuum damage theory—application to concrete. J Eng Mech 115(2):345–365

Min KB, Jing L (2004) Stress dependent mechanical properties and bounds of poisson's ratio for fractured rock masses investigated by a DFN-DEM technique. Int J Rock Mech Min Sci 41(3):431–432

Pariseau WG, Puri S, Schmelter SC (2008) A new model for effects of impersistent joint sets on rock slope stability. Int J Rock Mech Min Sci 45(2):122–131

Ramamurthy T, Rao GV, Singh J (1993) Engineering behaviour of phyllites. Eng Geol 33(3):209–225

Rao KS (1984) Strength and deformation behaviour of sandstones. PhD Thesis. Indian Institute of Technology, Delhi

Sahoo S (2011) A Study on strength and deformation behaviour of jointed rock mass. PhD thesis. Department of Civil Engineering, Indian Institute of Technology, Delhi

Singh M, Rao KS (2005) Empirical methods to estimate the strength of jointed rock masses. Eng Geol 77(1–2):127–137

Singh M, Samadhiya NK, Kumar A, Kumar V, Singh B (2015) A nonlinear criterion for triaxial strength of inherently anisotropic rocks. Rock Mech Rock Eng 48(4):1387–1405

Tang CA (1997) Numerical simulation on progressive failure leading to collapse and associated seismicity. Int J Rock Mech Min Sci 34(2): 249–261

Tang CA, Lin P, Wong RHC, Chau KT (2001) Analysis of crack coalescence in rock-like materials containing three flaws-part II: numerical approach. Int J Rock Mech Min Sci 38(7):925–939

Tang CA, Wong RHC, Chau KT, Lin P (2005) Modeling of compression-induced splitting failure in heterogeneous brittle porous solids. Eng Fract Mech 72(4):597–615

Tiwari RP, Rao KS (2007) Response of an anisotropic rock mass under polyaxial stress state. J Mater Civ Eng 19(5):393–403

Wang PT, Yang TH, Xu T, Cai MF, Li CH (2016) Numerical analysis on scale effect of elasticity, strength and failure patterns of jointed rock masses. Geosci J 20(4):1–11

Wang X, Jia Z, Zhang F, Li X (2010) The simulation of joint network and its application. China Water Power Press, Beijing

Weibull W (1951) A statistical distribution function of wide applicability. J Appl Mech 18:293–297

Wu Q, Kulatilake PHSW (2012) REV and its properties on fracture system and mechanical properties, and an orthotropic constitutive model for a jointed rock mass in a dam site in China. Comput Geotech 43(3):124–142

Wu ZJ, Fan LF, Liu QS, Ma GW (2017) Micro-mechanical modeling of the macro-mechanical response and fracture behavior of rock using the numerical manifold method. Eng Geol 225:49–60

Xu GW, He C, Su A, Chen ZQ (2018) Experimental investigation of the anisotropic mechanical behavior of phyllite under triaxial compression. Int J Rock Mech Min Sci 104:100–112

Xu T, Ranjith PG, Wasantha PLP, Zhao J, Tang CA, Zhu WC (2013) Influence of the geometry of partially-spanning joints on mechanical properties of rock in uniaxial compression. Eng Geol 167:134–147

Yan YL, Xu T, Zhang YJ, Wasantha PLP (2013) Numerical simulation of the effect of joint orientation on the failure strength of rock. Appl Mech Mater 477-478:5

Yang JP, Chen WZ, Yang DS, Yuan JQ (2015a) Numerical determination of strength and deformability of fractured rock mass by FEM modeling. Comput Geotech 64:20–31

Yang SQ, Jing HW (2011) Strength failure and crack coalescence behavior of brittle sandstone samples containing a single fissure under uniaxial compression. Int J Fract 168:227–250

Yang TH, Wang PT, Xu T, Yu QL, Zhang PH, Shi WH, Hu GJ (2015b) Anisotropic characteristics of jointed rock mass: a case study at shirengou iron ore mine in China. Tunn Undergr Space Technol 48:129–139

Zhang HH, Liu SM, Han SY, Fan LF (2018) Modeling of 2D cracked FGMs under thermo-mechanical loadings with the numerical manifold method. Int J Mech Sci 148:103–117

Zhang JC, Zhou SH, Xu XH, Fang LG (2013) Evolution of the elastic properties of a bedded argillite damaged in cyclic triaxial tests. Int J Rock Mech Min Sci 58(1):103–110

Zhang XP, Wong LNY, Wang SJ, Han GY (2011) Engineering properties of quartz mica schist. Eng Geol 121(3):135–149

Zhou JR, Wei J, Yang TH, Zhu WC, Li LC, Zhang PH (2018) Damage analysis of rock mass coupling joints, water and microseismicity. Tunn Undergr Space Technol 71:366–381

Zhu WC, Tang CA (2004) Micromechanical model for simulating the fracture process of rock. Rock Mech Rock Eng 37(1):25–56